25

Jets and Plumes*

Scott A. Socolofsky
Texas A&M University

Tobias Bleninger
Federal University of Paraná

Robert L. Doneker
MixZon, Inc.

25.1 Introduction 329
25.2 Principles 331
Governing Variables • Boundary Layer Approximation • Turbulence Closure: Entrainment Hypothesis
25.3 Methods of Analysis 333
Dimensional Analysis • Buoyant Jet Integral Models
25.4 Applications 341
Discharge Analysis Using CORMIX
25.5 Extensions for Multiport Diffusers 344
25.6 Challenges 347
References 347

25.1 Introduction

Turbulent buoyant jets are a fundamental flow class in the natural and engineered environment and span the full asymptotic range of jet and plume behavior: round jets, line jets, momentum puffs, negative jets, round plumes, line plumes, and thermals. In summary, buoyant jets occur whenever fluid is discharged with an excess of or deficit in momentum and/or buoyancy through a constriction into a receiving fluid body. They occur in a whole host of applications, and we would like to quote Gerhard Jirka from his (2004) paper in the journal *Environmental Fluid Mechanics* where he outlined his view of the topic:

> Buoyant jet motions (sometimes called forced plumes) are prevalent in the natural environment and in engineering applications. They are most spectacular in volcanic gas eruptions, they occur as hydrothermal vent flows in the deep ocean or as fresh groundwater plumes in the coastal zone. They are a key feature in society's fluid waste disposal methods, be it in the form of gaseous emissions into the atmosphere from industrial and domestic smokestacks, from mobile exhausts and from cooling towers, or of liquid releases into water bodies from industrial, municipal and agricultural sources or mining and oil extraction operations. They are an integral part of building ventilation and air conditioning systems. And they play a central role as mixing and injection devices in chemical reactors, waste and sewage treatment plants, desalination plants, combustion chambers, jet engines, or heat exchangers as well as stratification control and oxygenation devices in lakes or reservoirs.

In this chapter, we will focus our attention on the most common tools used to analyze buoyant jet behavior in the environment and highlight areas where research is ongoing.

Though the study and observation of buoyant jets began hundreds of years ago, the quantitative analysis of their behavior began in earnest with the introduction of the boundary layer theory by Prandtl and colleagues (Görler 1942; Tollmien 1926). Jirka (2004) presents a detailed history of turbulent buoyant jet analysis; here, we highlight some of the critical stages of development from his survey. Initial work employed similarity solutions based on different formulations of the Prandtl mixing length theory (see also Schlichting [1960] for a summary). The more generalized integral model approach began its development through the work of Reichardt (1941), who showed that the Gaussian profile was an acceptable approximation to the cross-sectional shape of the jet integral properties. Using this approximation, early models relied on a turbulent diffusion model for jet expansion until the seminal paper by Morton et al. (1956) who introduced Taylor's concept of jet entrainment. The entrainment model hypothesizes that jets grow by incorporating ambient fluid into the jet by turbulent motion and further that the inward velocity of the entraining fluid at the jet edge is proportional to a characteristic velocity scale in the jet, taken as the time-average centerline velocity. The advantage of the entrainment approach is in the robustness of its applicability, making it capable of modeling quite complicated flows, including ambient stratification and crossflow.

* *Handbook of Environmental Fluid Dynamics, Volume One*, edited by H. J. S. Fernando. © 2013 CRC Press/Taylor & Francis Group, LLC. ISBN: 978-1-4398-1669-1.

General buoyant jet models based on the entrainment hypothesis and capable of simulating several different source and ambient conditions later developed, initiated by the work of Fan (1967). This model development was also supplemented by the excellent dimensional analysis of Wright (1977), and a detailed summary of these early activities is presented in Fischer et al. (1979). A more recent historical perspective on the entrainment hypothesis is also presented in Turner (1986). Since then, models have been generalized (see, e.g., Doneker and Jirka 1991; Jirka 2004; Jirka and Doneker 1991) and have benefitted from a wide range of new validation data, particularly from laboratory methods utilizing particle image velocimetry (PIV) and laser-induced fluorescence (LIF) (see, e.g., Davidson and Pun 1999; Tian and Roberts 2003; Yu et al. 2006, and other chapters in this book).

While our understanding of turbulent buoyant jet behavior is becoming quite detailed, their analysis remains challenging due to the wide range of time and space scales involved in their dynamic evolution. Figure 25.1 presents an example laboratory experiment of a buoyant jet along with a summary of the scales involved in coastal wastewater discharges. In the near-field region, close to the source, the buoyant jet exhibits the canonical self-similarity behavior and jet entrainment. As the jet is either arrested by the stratification (as in Figure 25.1) or encounters a boundary (side walls, free surface, or reservoir bottom), it enters an intermediate regime of rapid spreading in which the boundary layer assumption critical to the turbulent jet analysis breaks down, and the flow is no longer classified as a buoyant jet. At the end of this spreading region, the discharge enters a far-field behavior, dominated by ambient currents, turbulent diffusion,

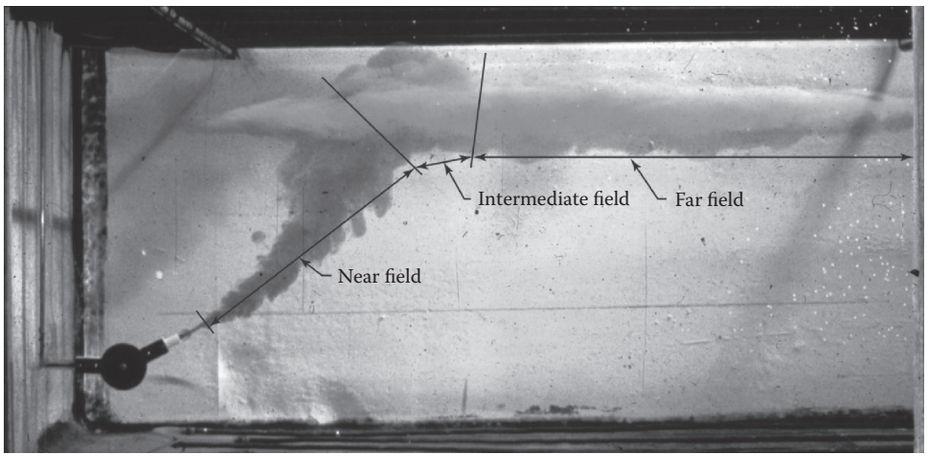

(a)

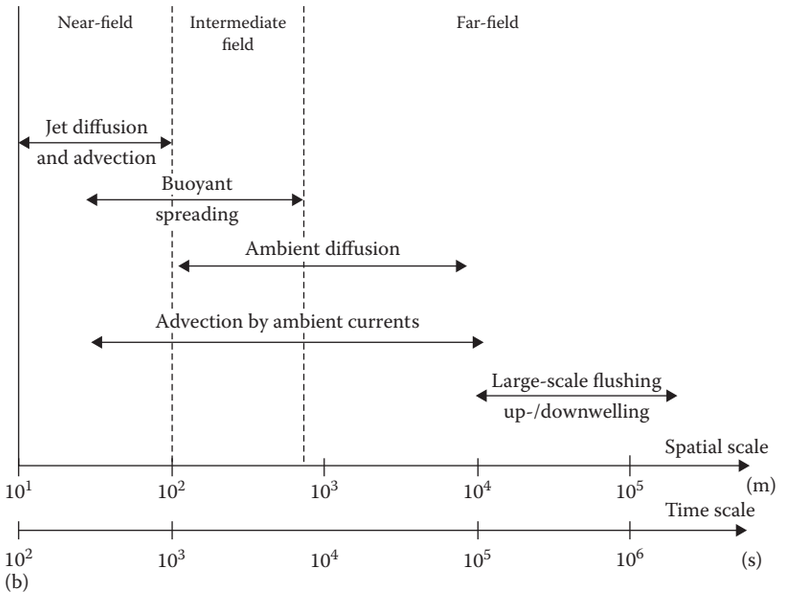

(b)

FIGURE 25.1 Laboratory experiment of an inclined, turbulent buoyant jet in a linearly stratified quiescent reservoir and a sketch of the characteristic length and time scales affecting coastal wastewater discharges.

and large, basin-scale motion. Because the height of rise of the plume and the initial dilution entering the far field is strongly affected by processes in the near-field, models of buoyant jet behavior are critical to the fate and transport modeling of environmental discharges. Hence, the near-field jet model is of fundamental importance.

In the remainder of this chapter, we present an overview of the methods used to analyze buoyant jets in the environment. The Principles section outlines the quantitative parameters used to describe buoyant jets and introduces the boundary layer approximation and the details of the entrainment hypothesis as it applies to turbulent buoyant jets. In the Methods of Analysis section, we begin with a discussion of dimensional analysis and the scaling relationships that have been developed for many asymptotic and transitional regimes of jet flow and conclude with a presentation of the governing equations for the integral model of a general turbulent buoyant jet in a flowing and density-stratified ambient reservoir. The Applications section highlights how such models are used in regulatory mixing zone analysis, particularly through the U.S. Environmental Protection Agency (EPA) model CORMIX, and introduces example extensions of the integral model to multiport diffusers and surface and bottom jets. The final section, Challenges, highlights several areas of ongoing research to improve and extend buoyant jet models for an ever increasing range of applications.

25.2 Principles

25.2.1 Governing Variables

Jets and plumes are typically described mathematically by a set of flux variables expressed in kinematic form. Figure 25.2 is a sketch of the general case of a buoyant jet discharged at an arbitrary angle (σ relative to the x-axis and θ relative to the horizontal plane) into a flowing and density-stratified ambient reservoir. For this case, the independent flux variables are the volume flux Q, momentum flux M, buoyancy flux J, and the mass flux of passive tracers Q_{ci}. Although J is the important forcing parameter for buoyancy, it is often more convenient to track the fluxes of the state variables X_i (e.g., heat, salinity, etc.) affecting the density and to compute the density from an equation of state of the form $\rho = f(X_i)$—once the density is known, it is substituted to compute the buoyancy flux J separately.

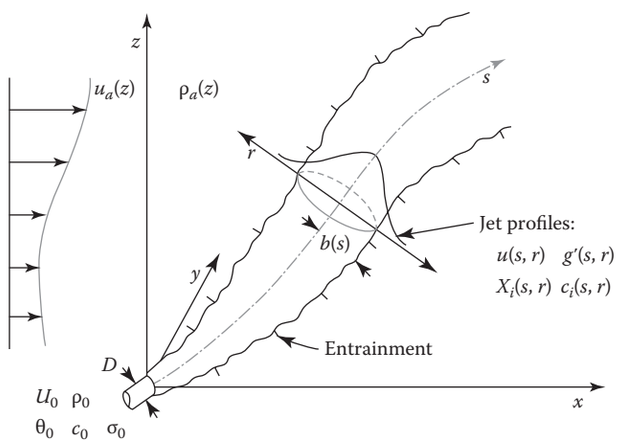

FIGURE 25.2 Schematic of a general round buoyant jet into a flowing and density-stratified ambient reservoir.

At the jet nozzle, these governing flux quantities are given by their initial values

$$Q_0 = U_0 a_0$$

$$M_0 = U_0 Q_0$$

$$J_0 = g_0' Q_0$$

$$Q_{Xi0} = X_{i0} Q_0$$

$$Q_{c_{i0}} = c_{i0} Q_0 \tag{25.1}$$

where

U_0 is the jet exit velocity

a_0 is the nozzle cross-sectional area (for round jets with pipe diameter D, $a_0 = (\pi/4)D^2$)

X_{i0} is the concentration of state variables in the effluent

c_{i0} is the concentration of passive tracers in the effluent

g_0' is the reduced gravity of the effluent, given by $g_0' = g(\rho_a - \rho_0)/\rho_r$, g is the acceleration of gravity, ρ_a is the ambient fluid density at the elevation of the jet exit, ρ_0 is the density of the effluent, ρ_r is a reference density, generally taken as a constant equal to the average density in the receiving fluid

The subscript "i" is used to keep track of multiple tracers

The values of these flux variables also evolve with distance from the nozzle along the jet trajectory s. This is true for both laminar and turbulent jets, though for turbulent jets, we average over an appropriate integral time scale to obtain statistically stationary results. The local flux variables can be computed by integrating profiles of velocity $u(s, r)$, reduced gravity $g'(s, r)$, and tracer concentrations $X_i(s, r)$ and $c_i(s, r)$ over the jet cross section (perpendicular to the jet axis). Thus, for a round jet, we obtain

$$Q(s) = 2\pi \int_0^\infty u(s,r) r dr$$

$$M(s) = 2\pi \int_0^\infty u^2(s,r) r dr$$

$$J(s) = 2\pi \int_0^\infty u(s,r) g'(s,r) r dr$$

$$Q_{Xi}(s) = 2\pi \int_0^\infty u(s,r) X_i(s,r) r dr$$

$$Q_{ci}(s) = 2\pi \int_0^\infty u(s,r) c_i(s,r) r dr \tag{25.2}$$

These variables form the state space of unknown quantities that are solved for by jet integral models. For line jets, the equations are similar, with the integrals taken over a Cartesian coordinate system and the results expressed as per unit length along the jet slot.

When the receiving fluid has non-zero values of some of the variables (as due to an ambient current or background tracer concentration), care must be taken to distinguish between the relative value in the jet compared to the background value. We have already seen this fact in the reduced gravity, which expresses the difference between ρ_a, the absolute density in the ambient fluid outside the jet at s, and $\rho(s, r)$, the absolute density in the jet: $g'(s,r) = g(\rho_a - \rho(s,r))/\rho_r$. Similarly, our interest is to solve for the excess velocity and concentration in the jet above the ambient value. Hence, we may express the local variables as

$$u(s,r) = u_j(s,r) + u_a$$

$$X_i(s,r) = X_{ij}(s,r) + X_{ia}$$

$$c_i(s,r) = c_{ij}(s,r) + c_{ia} \tag{25.3}$$

Here, the subscript "j" indicates the excess value in the jet and the subscript "a" indicates the value for the ambient reservoir outside the jet at s; for the vector velocity, we take u_a as the component along the jet axis.

Away from the nozzle, the buoyant jet is also described by characteristic values of its dynamic jet properties. These variables include the jet half-width $b(s)$ and centerline values of the velocity $u_c(s)$, reduced gravity $g'_c(s)$, and passive tracer concentrations $X_{ic}(s)$ and $c_{ic}(s)$. Because the cross-sectional profiles of the jet properties asymptotically approach zero, the half-width is usually defined as the lateral distance from the centerline to a point where the mean velocity is a fixed fraction of the average centerline velocity: $b = r(\delta u_c)$. Common values for δ are 1/2 or 1/e. Profiles of concentration are wider than that of velocity by a constant spreading factor λ, such that dissolved constituents have a width λb.

From these parameters describing the jet motion, an important property for environmental applications of jets and plumes known as the dilution S may also be derived, defined as the total volume of a sample divided by the volume of effluent in the sample. Several processes affect the effluent volume in the plume, including physical mixing, chemical transformation, and boundary interaction processes. In this chapter, we will focus on the pure hydrodynamic dilution, which for a conservative tracer (nonreacting) can be defined as

$$S_i = \frac{c_{i0}}{c_{ic}} \tag{25.4}$$

Because c_{ic} is a jet excess concentration, the dilution computed by this formula will give the true dilution of the effluent regardless of concentrations in the ambient reservoir.

25.2.2 Boundary Layer Approximation

Jets and plumes are among the canonical free shear flows that satisfy the boundary layer approximation, where the width of the jet is much less than the longitudinal length scale along the jet centerline. For an axisymmetric jet, the Reynolds averaged boundary layer equations are (refer to Figure 25.2)

$$\frac{\partial u}{\partial s} + \frac{1}{r}\frac{\partial rv}{\partial r} = 0 \quad \text{(Continuity equation)}$$

$$u\frac{\partial u}{\partial s} + v\frac{\partial u}{\partial r} = -\frac{1}{r}\frac{\partial}{\partial r}\left(r\overline{u'v'}\right)$$

$$\left(\text{Momentum equation along the jet axis}\right)$$

$$0 = \frac{\partial p}{\partial r} \quad \left(\text{Momentum equation perpendicular to jet axis}\right)$$

where u' and v' are the fluctuating turbulent velocities in the s and r directions, respectively. For a pure jet in a quiescent and uniform unbounded domain, the boundary conditions at $r = 0$ are $v = 0$ and $\partial u/\partial r = 0$ and at $r \to \infty$ are $u \to 0$ and $\overline{u'v'} \to 0$.

For certain simplified turbulence closure models, such as the Prandtl mixing length hypothesis with

$$\overline{u'v'} = \varepsilon \frac{\partial u}{\partial r} \tag{25.5}$$

where ε is a constant, similarity solutions can be found (see e.g., Kundu and Cohen 2008; Schlichting 1960). For more complicated situations, numerical solutions may be obtained using various advanced turbulence models. A simple, yet flexible third alternative is to convert the aforementioned system of partial differential equations to ordinary differential equations by integrating over the plume cross section using an assumed, self-similar shape of the local variables, yielding the integral model equations for the flux variables defined in the previous section. The general form of the integration for a round jet is $2\pi\int_0^\infty (\cdot) r dr$, and applying this operation to the continuity equation and using the boundary conditions gives

$$\frac{d}{ds}\left(2\pi \int_0^\infty u(z,r) r dr\right) = -2\pi v(s,r) r\Big|_{r=\infty} \tag{25.6}$$

The integral on the left-hand side of the equation is just $Q(s)$. The term on the right-hand side of the equation is not zero and introduces a turbulent closure problem through the fact that the solution for v depends on the turbulence model used in the momentum equation. This term is usually evaluated at the edge of the plume at $r = b$ since its contribution is essentially constant beyond this radius, and the velocity obtained there is called the entrainment velocity v_e directed toward the jet centerline ($-r$ direction), yielding

$$\frac{dQ}{ds} = 2\pi b v_e \tag{25.7}$$

as the continuity equation. To obtain an equation for the momentum flux, we combine the continuity and momentum equations and then integrate over the cross section to obtain (Kundu and Cohen 2008)

$$\frac{dM}{ds} = 0 \tag{25.8}$$

hence, the momentum flux is preserved for a pure jet experiencing no ambient forcing or boundary interaction.

25.2.3 Turbulence Closure: Entrainment Hypothesis

As we see in the previous section, the solution for the flow in a jet requires a turbulence closure model, either for the kinematic Reynolds stress $\overline{u'v'}$ or for an entrainment velocity v_e. Two popular closure models are the spreading and entrainment hypotheses. The spreading hypothesis is based on the experimental observation that the jet width grows linearly with distance from the source, so that

$$\frac{db}{ds} = \text{const} \tag{25.9}$$

This closure is particularly useful for analytical solutions based on Prandtl's mixing length theory. Schlichting (1960) explains that the mixing length l for a jet is proportional to the local width l/b = const and that this constant leads to the linear growth in the spreading hypothesis. With this model, the solution to the boundary layer equations takes the same form as the laminar solution, but with the molecular kinematic viscosity replaced by the turbulent viscosity ε = const, which may be obtained experimentally.

The second closure model, the entrainment hypothesis, leads to the same solution for a simple jet as the spreading hypothesis, but from a more mechanistic perspective, explaining the reason for the observed spreading. In the entrainment hypothesis, the entrainment velocity is assumed to depend on the turbulence intensity, which scales with the centerline velocity, resulting in the relationship

$$\frac{v_e}{u_c} = \alpha \tag{25.10}$$

where α is a constant, called the entrainment coefficient and which is obtained by experiment. Substituting this relationship in the continuity Equation 25.7 for the 1D integral model and using the definitions in (25.2) leads to a closed system of equations for Q and M.

The entrainment hypothesis has been shown to be a very robust relationship, valid from laboratory scales of a few centimeters up to geophysical scales of several kilometers, as created by volcanic eruptions (Turner 1986). Because of its physical interpretation as the inflow of ambient fluid along the edge of the jet, the entrainment hypothesis is also a much more flexible tool than the spreading hypothesis for developing models of more complicated jets involving forcing from ambient currents and stratification. It is also important to note that the entrainment hypothesis is a turbulence closure model; hence, it is only appropriate for turbulent jets and plumes, at a Reynolds number based on the jet width above about 500.

25.3 Methods of Analysis

The three classes of methods for buoyant jet flows used to solve for the governing parameters described earlier are *empirical*, *integral*, and *numerical* methods. The empirical methods are introduced in the following in the Dimensional Analysis section, followed by the integral methods in the section on Buoyant Jet Integral Models. These methods are generally adequate for each of the asymptotic flow regimes defined in the introduction (e.g., pure jet, pure plume, momentum puff, etc.) and in gradual transitions among these regimes.

For highly complex situations, such as nontrivial jet merging processes, unsteady flow analysis, complex discharge geometries, and boundary interactions, numerical solutions are required using advanced (at least two equation) turbulence closures. As distinct from the empirical or integral approach, numerical solutions calculate all flow characteristics at every point of the flow domain, thus they need to resolve the entire jet-induced velocity field and its interaction with the surrounding fluid. For the buoyant jet, the hydrodynamic and constituent transport equations are dynamically coupled. In addition, the sharp gradients and small scales in the jet near field require nondispersive numerical schemes for the convective terms and specialized turbulence closure models. For the same reasons, grid generation and computations are time-consuming, limiting the opportunity to apply numerical solutions to many designs. Furthermore, uncertainties exist in prescribing appropriate boundary conditions for the ambient flow, and calibration is needed for the parameters of the turbulence model, limiting the predictive capabilities of these models (Xiao et al. 2005); thus,

a more detailed discussion of computational fluid dynamics models applied to jets and plumes is beyond the scope of this chapter. We will show, however, that the empirical and integral solutions are adequate for the design of most single and multiport discharges in the environment.

25.3.1 Dimensional Analysis

Because of the self-similarity behavior of the asymptotic types of the buoyant jet, dimensional analysis is a powerful tool to both predict relationships among the governing variables and to classify buoyant jet flows into different asymptotic regimes.

As an example of empirical solutions to the jet flow, consider a pure jet discharging horizontally in the x-direction in a stagnant, uniform ambient reservoir. The local unknown quantities (dependent variables) are the velocities u and v, and the concentration of passive tracer c. Characteristic scales of interest that evolve along the jet trajectory are $b(x)$, $u_c(x)$, $Q(x)$, and $S_c(x)$, each a different function of several independent variables, (x, M_0, a_0, etc.). Dimensional analysis for a round jet then results in the parameters

$$\frac{b}{x} = k_1, \quad \frac{u_c x}{\sqrt{M_0}} = k_2, \quad \frac{Q}{\sqrt{M_0 x}} = k_3, \quad \frac{S_c Q_0}{\sqrt{M_0 x}} = k_4 \tag{25.11}$$

The width b evolves following a linear dependence on x with the proportionality factor $k_1 = 0.11$, determined by experiments (Jirka 2004), and the centerline velocity decays inversely with the distance with the proportionality factor $k_2 = 7.25$ (Jirka 2004). The flow rate and dilution increase linearly with distance (from experiments $k_3 = 0.27$, and $k_4 = 0.1623$; Jirka 2004).

Because of the self-similarity of the flow, these four constants can also be expressed in terms of two other experimental constants, an entrainment coefficient $\alpha_{jet} = 0.055$, and a tracer spreading rate $\lambda_{jet} = 1.20$, yielding

$$k_1 = 2\alpha_{jet}, \quad k_2 = \frac{1}{\sqrt{2\pi}\alpha_{jet}}, \quad k_3 = 2\sqrt{2\pi}\alpha_{jet},$$
$$k_4 = \frac{\lambda_{jet}^2}{1+\lambda_{jet}^2}\frac{2\sqrt{2\pi}\alpha_{jet}}{1+\lambda_{jet}^2} \tag{25.12}$$

Similar analysis is possible for other jet properties and each of the asymptotic buoyant jet regimes. These are summarized in Table 25.1. However, with increasing complexity, the number of independent parameters increases, and difficulties arise in defining consistent relations on the one hand and elaborating necessary laboratory studies on the other. Thus, correlation equations resulting from dimensional analysis are restricted to steady asymptotic cases with some slight extensions.

As a second example of dimensional analysis, we consider more complicated cases and attempt to classify regimes of the flow as, for instance, jet, plume, crossflow, or stratification dominated, among others. Consider the jet of the previous example with the added effect of an initial buoyancy flux. Early attempts to predict the trajectory of a buoyant jet used the exit geometry as the important scales to nondimensionalize the data. However, as shown in the left plot of Figure 25.3, this scaling is unable to collapse the data, and different lines are obtained for different initial Froude numbers

$$F_0 = \frac{U_0}{\sqrt{g_0' D_0}} \tag{25.13}$$

Instead of the nozzle exit, another characteristic length scale for the jet can be defined that accounts for differences in the initial Froude number, by taking a ratio of the initial momentum and buoyancy fluxes yielding

$$L_M = \frac{M_0^{3/4}}{J_0^{1/2}} \tag{25.14}$$

When applied to predict the buoyant jet trajectory, this new scale efficiently collapses the data to a single line (right plot of Figure 25.3). Because L_M is a measure of the length scale of the jet-dominated region of a buoyant discharge, it also allows distinguishing the jet-dominated region of more complicated flows, as illustrated in Figure 25.4 and expanded in Section 25.4.1.

A consistent length-scale-based categorization of the different buoyant jet regimes in the presence of crossflow and/or stratification is summarized in Fischer et al. (1979) and modified by Jirka and Akar (1991), giving the following length scales:

- $L_M = M_0^{3/4}/J_0^{1/2}$: The jet to plume transition length scale, which denotes a scaling for the transition from jet to plume behavior in a stagnant ambient (note that the product $D_0 F_0$ is proportional to L_M).
- $L_m = M_0^{1/2}/u_a$: The jet to crossflow length scale, which denotes a scaling for the distance of transverse jet penetration beyond which strong deflection by the crossflow occurs.
- $L_b = J_0/u_a^3$: The plume to crossflow length scale, which denotes a scaling for the distance of plume penetration beyond which strong deflection by the crossflow occurs.
- $L_b' = J_0^{1/4}/\varepsilon^{3/4}$: The plume to stratification length scale, which denotes a scaling for the distance at which the jet becomes strongly affected by the stratification (defined by $\varepsilon = -(g/\rho_r)(d\rho_a/dz)$, the ambient buoyancy gradient), leading to terminal layer formation and horizontally spreading in a stagnant linearly stratified ambient.

For a comprehensive discussion of these and other scales for buoyant jet classification, see Jirka and Doneker (1991). Similar analyses for the dilution of a buoyant jet in quiescent, flowing, and stratified ambient reservoirs is presented in Fischer et al. (1979) and Jirka and Lee (1994).

TABLE 25.1 Equations for the Five Self-Similar Asymptotic Regimes of the Round Buoyant Jet

Regime (All $\lambda = 1.20$)	Width b	Centerline Velocity u_c or Trajectory Elevation z	Volume Flux Q	Centerline Dilution $S_c = c_o/c_c$	Remarks
Jet	$b = 2\alpha_{jet}x$	$u_c = \frac{1}{\sqrt{2\pi}\,\alpha_{jet}}\frac{M_o^{1/2}}{x}$	$Q = \sqrt{2\pi}\,2\alpha_{jet}M_o^{1/2}x$	$S_c = \frac{\lambda^2}{1+\lambda^2}\frac{\sqrt{2\pi}2\alpha_{jet}}{1+\lambda^2}\frac{M_o^{1/2}x}{Q_o}$	Assumes discharge in x-direction
$\alpha_{jet} = 0.055$	$b = 0.11x$	$u_c = 7.25\frac{M_o^{1/2}}{x}$	$Q = 0.27M_o^{1/2}x$	$S_c = 0.162\frac{M_o^{1/2}x}{Q_o}$	
Plume	$b = \frac{6}{5}\alpha_{plume}z$	$u_c = \frac{1}{2}\left(\frac{25}{3\pi}\frac{1+\lambda^2}{\alpha_{plume}^2}\right)^{1/3}\frac{J_o^{1/3}}{z^{1/3}}$	$Q = \frac{6}{5}\left(\frac{9}{5}(1+\lambda^2)\pi^2\alpha_{plume}^4\right)^{1/3}J_o^{1/3}z^{5/3}$	$S_c = \frac{\lambda^2}{1+\lambda^2}\frac{6}{5}\left(\frac{9}{5}\frac{\lambda^6}{(1+\lambda^2)^2}\pi^2\alpha_{plume}^4\right)^{1/3}\frac{J_o^{1/3}z^{5/3}}{Q_o}$	
$\alpha_{plume} = 0.083$	$b = 0.10z$	$u_c = 4.9\frac{J_o^{1/3}}{z^{1/3}}$	$Q = 0.152J_o^{1/3}z^{5/3}$	$S_c = 0.090\frac{J_o^{1/3}z^{5/3}}{Q_o}$	
Wake	$b = \left(\frac{3\alpha_{wake}}{2\pi}\right)^{1/3}\frac{M_{oe}^{1/3}x^{1/3}}{u_a^{2/3}}$	$u_c = \frac{1}{\pi}\left(\frac{2\pi}{3\alpha_{wake}}\right)^{2/3}\frac{M_{oe}^{1/3}u_a^{1/3}}{x^{2/3}}$	$Q = 2\pi\left(\frac{3\alpha_{wake}}{2\pi}\right)^{2/3}\frac{M_{oe}^{2/3}x^{2/3}}{u_a^{1/3}}$	$S_c = \lambda^2\pi\left(\frac{3\alpha_{wake}}{2\pi}\right)^{2/3}\frac{M_{oe}^{2/3}x^{2/3}}{u_a^{1/3}Q_o}$	
$\alpha_{wake} = 0.11$	$b = 0.37\frac{M_{oe}^{1/3}x^{1/3}}{u_a^{2/3}}$	$u_c = 2.27\frac{M_{oe}^{1/3}u_a^{1/3}}{x^{2/3}}$	$Q = 0.88\frac{M_{oe}^{2/3}x^{2/3}}{u_a^{1/3}}$	$S_c = 0.63\frac{M_{oe}^{2/3}x^{2/3}}{u_a^{1/3}Q_o}$	
Advected Line Puff	$b = \left(\frac{3\alpha_{puff}}{4\pi}\right)^{1/3}\frac{M_{ot}^{1/3}x^{1/3}}{u_a^{2/3}}$	$z = \left(\frac{6}{\pi\alpha_{puff}^2}\right)^{1/3}\frac{M_{ot}^{1/3}x^{1/3}}{u_a^{2/3}}$	$Q = \left(\sqrt{\frac{\pi}{2}}3\alpha_{puff}\right)^{2/3}\frac{M_{ot}^{2/3}x^{2/3}}{u_a^{1/3}}$	$S_c = \frac{\lambda^2}{2}\left(\sqrt{\frac{\pi}{2}}3\alpha_{puff}\right)^{2/3}\frac{M_{ot}^{2/3}x^{2/3}}{u_a^{1/3}Q_o}$	Assumes transverse momentum flux M_{ot} in z-direction
$\alpha_{puff} = 0.5$	$b = 0.49\frac{M_{ot}^{1/3}x^{1/3}}{u_a^{2/3}}$	$z = 1.96\frac{M_{ot}^{1/3}x^{1/3}}{u_a^{2/3}}$	$Q = 1.52\frac{M_{ot}^{2/3}x^{2/3}}{u_a^{1/3}}$	$S_c = 1.10\frac{M_{ot}^{2/3}x^{2/3}}{u_a^{1/3}Q_o}$	
Advected Line Thermal	$b = \left(\frac{3\alpha_{thermal}}{8\pi\lambda}\right)^{1/3}\frac{J_o^{1/3}x^{2/3}}{u_a}$	$z = \left(\frac{3}{\pi\lambda\alpha_{thermal}^2}\right)^{1/3}\frac{J_o^{1/3}x^{2/3}}{u_a}$	$Q = \left(\sqrt{\frac{\pi}{2}}\frac{3\alpha_{thermal}}{2\lambda}\right)^{2/3}\frac{J_o^{2/3}x^{4/3}}{u_a}$	$S_c = \frac{\lambda^2}{2}\left(\sqrt{\frac{\pi}{2}}\frac{3\alpha_{thermal}}{2\lambda}\right)^{2/3}\frac{J_o^{2/3}x^{4/3}}{u_aQ_o}$	
$\alpha_{thermal} = 0.5$	$b = 0.37\frac{J_o^{1/3}x^{2/3}}{u_a}$	$z = 1.47\frac{J_o^{1/3}x^{2/3}}{u_a}$	$Q = 0.85\frac{J_o^{2/3}x^{4/3}}{u_a}$	$S_c = 0.61\frac{J_o^{2/3}x^{4/3}}{u_aQ_o}$	

Source: Reproduced from Jirka, G.H., *Environ. Fluid Mech.*, 4(1), 1–56, 2004.

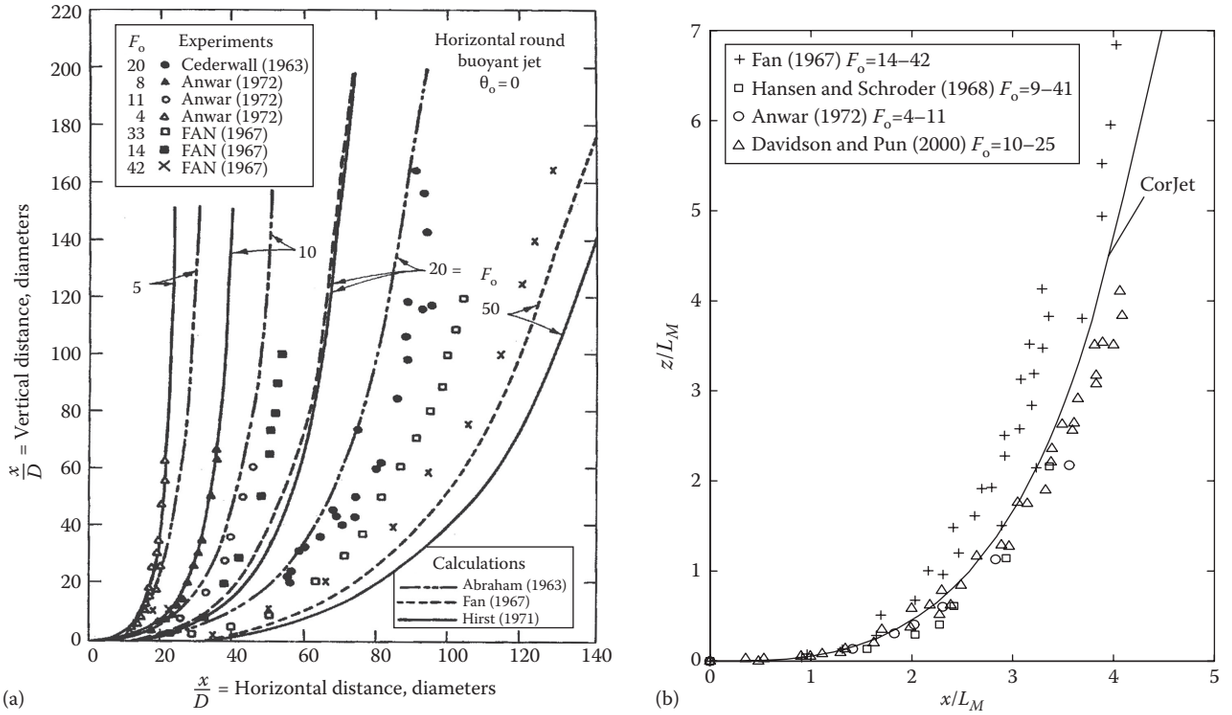

FIGURE 25.3 Three-dimensional horizontal buoyant jet trajectories for a single-port discharge into a stagnant reservoir. Comparison between predictions and experimental data. (a) normalized with port diameter. (b) Normalized with the momentum length scale L_M. (Reproduced from Jirka, G.H., *Environ. Fluid Mech*., 4(1), 1–56, 2004. With permission.)

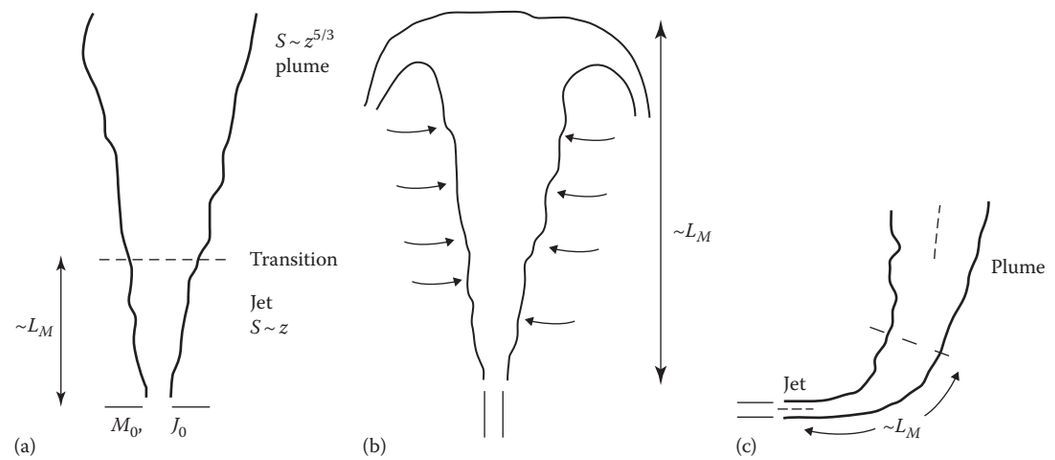

FIGURE 25.4 Schematic representation of the jet length scale L_M for (a) a vertical buoyant jet in an unstratified ambient reservoir, (b) a vertical buoyant jet in stratification, and (c) a horizontal buoyant jet.

25.3.2 Buoyant Jet Integral Models

For the design and more detailed analysis of real discharges in the environment, integral jet models are the most common tools for predicting the evolution in the near field. Strictly speaking, these tools are based on the similarity assumption: profiles of velocity, concentration, and other jet properties have the same shapes at all heights; only their magnitudes change. Self-similarity is valid in unbounded domains where there is no characteristics length scale for the flow. Stratification, crossflows, and the existence of lateral (side-walls) and horizontal (bottom and free-surface) boundaries all act to introduce external length

scales to the problem and break down the self-similarity of the jet. Nonetheless, because of the robustness of the entrainment hypothesis, acceptable results may be obtained in most of these situations provided experimental data are used to validate their accuracy and range of applicability.

In addition to self-similarity, the buoyant jet integral equations derived here are constrained by a few other assumptions. Their derivation starts with the Reynolds averaged Navier-Stokes equations and applies the boundary layer approximation; hence, the fluids must be Newtonian, the flow must be thin in lateral extent compared to distance along the flow path, and the results should be interpreted as time averages over the turbulent fluctuations. Jirka (2004) summarized the implications of these limitations in six principles that must be met by any jet integral model to obtain a reasonably accurate solution. Briefly, for a round jet, these are as follows:

1. Solutions are valid only for the five asymptotic conditions exhibiting strict self-similarity, a constant internal force balance, and invariant turbulence properties. These are the pure jet, pure plume, pure wake, advected line puff, and advected line thermal. As a corollary, all jet integral models must be validated to show that they accurately reproduce these five asymptotic regimes.
2. Models of the transitions among these five asymptotic solutions are arbitrary (they cannot be derived from first principles) and should be guided by good model agreement with available data.
3. Model solutions cannot be trusted when the boundary layer assumption is violated. This occurs whenever the jet undergoes strong spreading (as in the arrest due to ambient stratification) or strong curvature (as in jets directed into an opposing ambient current).
4. The initial zone of flow establishment (ZOFE) lacks self-similarity (the velocity profile shape transitions from top-hat pipe profiles to the Gaussian jet profile); hence, the ZOFE should not be modeled by the jet integral equations. Instead, empirical relations in this region (extended 5–10 times the exit diameter) should be used to establish an equilibrium initial condition for the jet integral model at the end of the ZOFE.
5. The jet integral equations should be formulated in terms of the flux quantities (Q, M, J, etc.) because these quantities are conservative and generally do not exhibit strong changes or singularities as some of the local variables do (e.g., b, u, g', etc.). This principle acts to preserve solution accuracy.
6. The model formulation must be accompanied by limits of applicability. In particular, the model must terminate when boundary interactions occur or the flow transitions to an intermediate- or far-field behavior dominated by turbulent diffusion over entrainment-related spreading.

One integral model that meets each of these principles is the CorJet module as implemented in the CORMIX system for the analysis of regulatory mixing zones (Doneker and Jirka 1991; Jirka 2004; Jirka and Doneker 1991; see also the Application section of this chapter). In the following, we derive the fundamental equations solved by this model and presented in Jirka (2004).

25.3.2.1 Coordinate System

Here, we derive the jet integral equations in an Eulerian sense along the jet centerline. Figure 25.5 shows a sketch of the jet trajectory and overlaying coordinate systems. The local, cylindrical coordinate system (s, r) is fixed to the jet trajectory, with s tangent to the local jet centerline and r the radial coordinate from s. The (s, r) coordinate system is also mapped to the fixed, Cartesian coordinate system (x, y, z), in which x points in the direction of the ambient current $\vec{u}_a = (u_a(z), 0, 0)$, z points opposite to the gravity vector $\vec{f}_g = (0, 0, -g)$, and the origin is at the jet exit (CORMIX solves for the more general case of a 2D, planar velocity field; however, we limit this chapter to the simplified

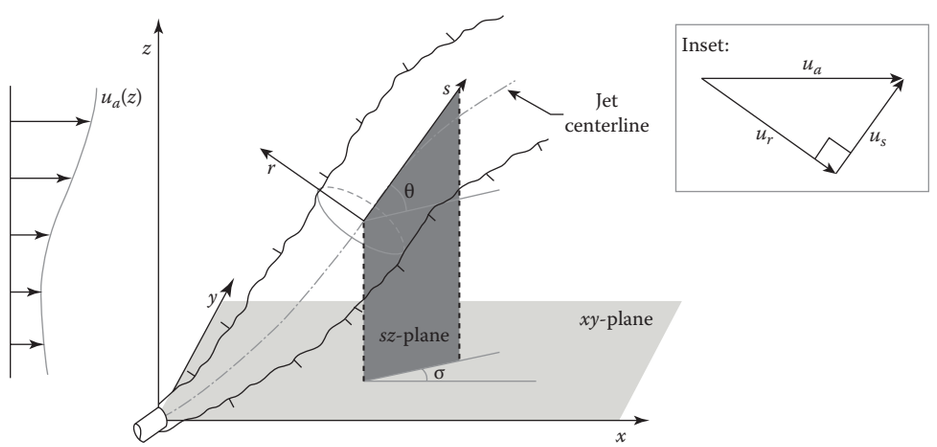

FIGURE 25.5 Schematic of the local (s, r) and fixed Cartesian (x, y, z) coordinate system for the buoyant jet integral model.

case defined here). A transform between the two coordinate systems is also depicted in the figure, where σ is the angle between the *s*- and *x*-axes, and θ is the angle between the *s*- and *z*-axes. Thus, a unit vector in the *s*-direction at the origin of the (*x*, *y*, *z*) AQ1 coordinate system has Cartesian coordinates

$$e_s = (\cos\sigma\cos\theta, \sin\sigma\cos\theta, \sin\theta) \tag{25.15}$$

Because entrainment fluxes into the jet are perpendicular to the *s*-axis in the model, an important quantity is the component of the ambient velocity vector transverse to *s*. Because $\vec{u}_a$ depends on *z* only, the projection of $\vec{u}_a$ on *s* is obtained by $u_s = \vec{u}_a \cdot e_s = u_a(z)\cos\sigma\cos\theta$. Then, the ambient velocity component transverse to *s* is found using the Pythagorean theorem (see inset in Figure 25.5), yielding

$$u_t = u_a\sqrt{1-\cos^2\sigma\cos^2\theta} \tag{25.16}$$

These and similar geometric transforms are used throughout the equations given in the following.

25.3.2.2 Lateral Profiles of the Local Variables

The choice of the shape of the lateral profiles for velocity, concentration, etc. is essentially arbitrary—square, so-called top-hat profiles perform equally well to more realistic profile shapes—because the model tracks only the flux resulting from an integral over the profile shape. Here, we use Gaussian profiles, both for their ease of use and because they most closely match the experimental data. We will develop the model for the general case of a stratified, flowing ambient condition, as sketched in Figure 25.5. For this model, Gaussian profiles give (Jirka 2004)

$$u(s,r) = u_c(s)\exp\left(-\frac{r^2}{b^2}\right) + u_a(z)\cos\sigma\cos\theta,$$

$$g'(s,r) = g'_c(s)\exp\left(-\frac{r^2}{(\lambda b)^2}\right)$$

$$X_i(s,r) = X_{ic}(s)\exp\left(-\frac{r^2}{(\lambda b)^2}\right) + X_{ia}(z),$$

$$c_i(s,r) = c_{ic}(s)\exp\left(-\frac{r^2}{(\lambda b)^2}\right) + c_{ia}(z)$$

where the centerline quantities are jet excess quantities above their ambient values.

25.3.2.3 Flux Equations

The state space of model fluxes are obtained by substituting these profiles into Equation 25.2 to obtain

$$Q(s) = 2\pi\int_0^\infty u(s,r)rdr = \pi b(s)^2(u_c(s) + 2u_a(z)\cos\sigma\cos\theta) \tag{25.17}$$

$$M(s) = 2\pi\int_0^\infty u(s,r)^2 rdr = \frac{1}{2}\pi b(s)^2(u_c(s) + 2u_a(z)\cos\sigma\cos\theta)^2 \tag{25.18}$$

$$Q_{Xi}(s) = 2\pi\int_0^\infty u(s,r)(X_i(s,r) - X_{ia}(z))rdr$$

$$= \pi b(s)^2\left(u_c(s)\frac{\lambda^2}{1+\lambda^2} + \lambda^2 u_a(z)\cos\sigma\cos\theta\right)X_{ic}(s) \tag{25.19}$$

$$Q_{ci}(s) = 2\pi\int_0^\infty u(s,r)(c_i(s,r) - c_{ia}(z))rdr$$

$$= \pi b(s)^2\left(u_c(s)\frac{\lambda^2}{1+\lambda^2} + \lambda^2 u_a(z)\cos\sigma\cos\theta\right)c_{ic}(s) \tag{25.20}$$

So far we have shown explicitly the dependence of each variable on *s* and *r*. After integrating as done earlier, the model unknowns become 1D along *s*; hence, we will drop this notation going forward and all flux and local variables may be assumed to depend on *s* only.

25.3.2.4 Model Conservation Equations

Figure 25.6 shows a sketch of a differential control volume along the jet trajectory for which we will derive the model equations. Flux quantities *F* enter the element at face 1 and exit at face 2. Ambient fluid is entrained along the sides of the jet with effective entrainment flow rate *E* per unit height. And the forces acting on the control volume are the drag force f_d due to the crossflow

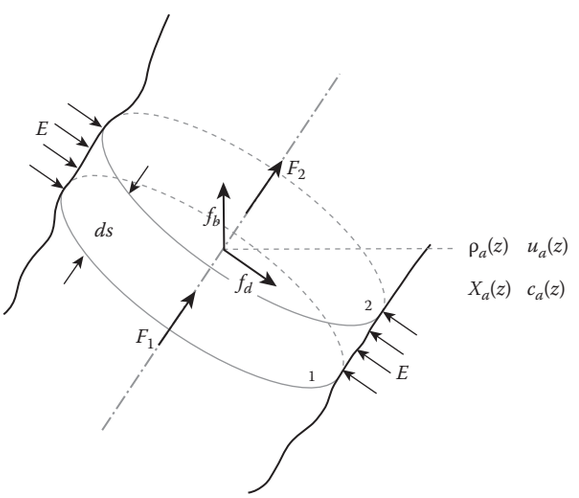

FIGURE 25.6 Schematic of the control volume of the buoyant jet used to derive the governing conservation equations of the integral jet model.

and the net buoyancy f_b of the control volume. The model equations are obtained by applying conservation laws to this control volume.

The entrainment rate E accounts for several shear mechanisms that result in entrainment of ambient fluid into the body of the turbulent buoyant jet. Similar mechanisms are at work in each of the asymptotic flow regimes (principle 1), and a general model is sought that accounts for an appropriate transition among these asymptotic solutions (as required by principle 2). Jirka (2004) suggests a general entrainment model of the form

$$E = 2\pi b(\alpha_e u_c + \alpha_4 \left|\cos\sigma\cos\theta\right| u_t) \tag{25.21}$$

The term $2\pi b$ is the local circumference of the jet. The first term in (25.21) accounts for the entrainment from jets, plumes and wakes, and an acceptable empirical model to achieve smooth transition among these asymptotic regimes is suggested by Jirka (2004) as

$$\alpha_e = \alpha_1 + \alpha_2 \frac{\sin\theta}{F_l^2} + \alpha_3 \frac{u_a \left|\cos\sigma\cos\theta\right|}{u_c + u_a} \tag{25.22}$$

The first term in (25.22) gives the entrainment coefficient for a pure jet, the second term adds the effect of the pure plume, and the third term incorporates the effect of the pure wake. The plume contribution is shown by experiment to depend on the local densimetric Froude number $F_l = u_c/\sqrt{g_c' b}$ and the vertical angle θ since buoyancy acts in the vertical direction. The wake effect is proportional to the wake parameter $u_a/(u_c + u_a)$ and the projection of the jet velocity on the x axis since the wake propagates in the direction of the ambient current (x-direction). The final term in the entrainment model (25.21) accounts for line puffs and thermals: the entrainment velocity is proportional to the ambient velocity transverse to the jet and the entrainment contribution depends on the component of the jet velocity in the ambient current direction: $\left|\cos\sigma\cos\theta\right|$. Hence, vertically oriented buoyant jets are dominated by jet and plume entrainment while the wake and crossflow entrainment mechanisms dominate as the jet bends over and transitions to a buoyant line thermal. Although crossflow entrainment is zero for the vertical jet ($\cos\theta = 0$ for $\theta = \pi/2$), the plume still bends over as regular jet entrainment engulfs ambient fluid having x-direction momentum and as the jet experiences a drag force in the x-direction.

The conservation of mass is obtained by a volume balance on the flows into and out of the control volume, giving

$$Q_2 - Q_1 = dQ = Eds \tag{25.23}$$

or, rearranging:

$$\frac{dQ}{ds} = E \tag{25.24}$$

Likewise, the conservation of mass for the state parameters and passive tracers are a simple flux balance over the control volume. However, because the flux variables are calculated in terms of the excess concentration, there are a few more steps. Consider the conservation of mass for the state variables over the control volume

$$\frac{d}{ds}\int X_i u dA = EX_{ia} \tag{25.25}$$

To arrange this equation in terms of concentration excess, substitute the conservation of volume Equation 25.26 to replace E in (25.25), giving

$$\frac{d}{ds}\int X_i u dA = X_{ia}\frac{d}{ds}\int u dA \tag{25.26}$$

We use the product rule on the right-hand side to bring X_{ia} into the derivative

$$\frac{d}{ds}\int X_i u dA = \frac{d}{ds}\left[X_{ia}\int u dA\right] - \frac{dX_{ia}}{ds}\int u dA \tag{25.27}$$

and bringing the first two terms of (25.27) together on the left-hand side of the equation to obtain

$$\frac{d}{ds}\left[\int X_i u dA - X_{ia}\int u dA\right] = -\frac{dX_{ia}}{ds}\int u dA \tag{25.28}$$

It is now possible to bring X_{ia} inside the integral in the second term of (25.28) since the integration is over r and not z or s. On the right-hand side we also apply the chain rule to dX_{ia}/ds and substitute $\int u dA = Q$, yielding

$$\frac{d}{ds}\int (X_i - X_{ia}) dA = -Q\frac{dX_{ia}}{dz}\sin\theta \tag{25.29}$$

We now recognize the quantity inside the integral as the mass flux of the excess concentration; hence,

$$\frac{dQ_{Xi}}{ds} = -Q\frac{dX_{ia}}{dz}\sin\theta \tag{25.30}$$

By similar algebra, the conservation equation for passive tracers gives

$$\frac{dQ_{ci}}{ds} = -Q\frac{dc_{ia}}{dz}\sin\theta \tag{25.31}$$

The advantage of the excess concentration formulation is that a simple equation for conservation of buoyancy is obtained when

the equation of state can be linearized (see, e.g., Jirka 2004). When the ambient concentration of passive tracers is zero, the concentration of tracer mass flux simply becomes

$$\frac{dQ_{ci}}{ds} = 0 \tag{25.32}$$

To derive the momentum equation, we require expressions for the forces acting on the control volume. The buoyancy contribution is the net reduced gravity across the centroid of the control volume, giving

$$f_b = 2\pi \int_0^\infty g'(s,r) r dr = \pi(\lambda b)^2 g'_c \tag{25.33}$$

in kinematic force per unit length dimensions, acting exclusively in the z-direction. The drag force is formulated in analogy to the drag around a cylinder of diameter $2\sqrt{2}b$ using the velocity transverse to s as the characteristic scale; hence,

$$\left|\vec{F}_d\right| = \frac{1}{2} c_D 2\sqrt{2} b u_a^2 (1 - \cos^2\sigma \cos^2\theta) \tag{25.34}$$

and the F_d vector is assumed to act in the same direction as the transverse velocity u_t. Decomposing the drag force into (x, y, z) components yields

$$\vec{f}_d = \left|\vec{F}_d\right| \left(\sqrt{1 - \cos^2\sigma \cos^2\theta}, \quad -\frac{\sin\sigma \cos\sigma \cos^2\theta}{\sqrt{1 - \cos^2\sigma \cos^2\theta}}, \right.$$
$$\left. -\frac{\sin\sigma \cos\sigma \cos\theta}{\sqrt{1 - \cos^2\sigma \cos^2\theta}} \right) \tag{25.35}$$

To test this formulation, consider three simple cases:

1. For a vertical buoyant jet, $\theta = \pi/2$ and $\sigma = 0$ so that the drag force acts in the x-direction, causing the plume to bend over.
2. For a horizontal jet with centerline along the x-axis, $\theta = 0$ and $\sigma = 0$. Here, the transverse velocity is zero; thus, F_d is zero. If the jet deviates slightly in the y-direction so that σ is small, the drag force is small, but almost all of it is directed in the negative y-direction; hence, causing the jet to correct its path and move back to the x-axis.
3. For a horizontal jet with centerline along the y-axis, $\theta = 0$ and $\sigma = \pi/2$, the drag force is large and is directed solely in the x-direction, similar to case 1.

With these forces, the conservation of momentum flux in the x-, y-, and z-directions follows from Newton's first law as (Jirka 2004)

$$\frac{d(M \cos\sigma \cos\theta)}{ds} = Eu_a + \left|\vec{F}_D\right| \sqrt{1 - \cos^2\sigma \cos^2\theta} \tag{25.36}$$

$$\frac{d(M \sin\sigma \cos\theta)}{ds} = -\left|\vec{F}_D\right| \frac{\sin\sigma \cos\sigma \cos^2\theta}{\sqrt{1 - \cos^2\sigma \cos^2\theta}} \tag{25.37}$$

$$\frac{d(M \sin\theta)}{ds} = \pi(\lambda b)^2 g'_c - \left|\vec{F}_D\right| \frac{\cos\sigma \cos\theta \sin\theta}{\sqrt{1 - \cos^2\sigma \cos^2\theta}} \tag{25.38}$$

where the term Eu_a accounts for the change in momentum due to entrainment of ambient fluid with velocity u_a in the x-direction and the other terms on the right-hand side of the equations are buoyancy and drag contributions.

To close the system of equations, the trajectory is obtained from

$$\frac{dx}{ds} = \cos\sigma \cos\theta \tag{25.39}$$

$$\frac{dy}{ds} = \sin\sigma \cos\theta \tag{25.40}$$

$$\frac{dz}{ds} = \sin\theta \tag{25.41}$$

and the density necessary to compute the reduced gravity is obtained from the equation of state.

25.3.2.5 Values of the Empirical Coefficients

To solve the model equations presented earlier, values for the five model parameters are required. These are obtained by validation to available data, and because of the robustness of the similarity solution, are constant over a very wide range of physical scales and also in many transition states between asymptotic flow solutions. Jirka (2004) reports the values used in CorJet as

$$\alpha_1 = 0.055, \quad \alpha_2 = 0.6, \quad \alpha_3 = 0.055, \quad \alpha_4 = 0.5 \tag{25.42}$$

$$\lambda = 1.20, \quad c_D = 1.3 \tag{25.43}$$

It is important to note here that these values depend on the shape of the lateral profiles (these values are for Gaussian profiles) and the chosen definition of the plume half-width b (taken as $1/e$ for the entrainment coefficients). Models using other profiles or definitions may result in the same solution as this model, but using different values for these five model parameters.

25.3.2.6 Validation

Integral models based on the equations presented earlier have been validated to all of the asymptotic regimes as well as many transition

cases in which different parts of the jet trajectory are dominated by different asymptotic dynamics, as in a buoyant jet transitioning to a plume. The purpose of model validation is both to check the accuracy of the numerical routines and computer code to ensure that the right equations are solved well and to check that the governing equations are indeed an adequate representation of the jet physics. In this section we highlight a few of the validation cases that have been applied to the CorJet model. For a more comprehensive suite of validation data, please see Jirka (2004).

1. *Pure jet*: The pure jet has no ambient density stratification or crossflow, and the effluent is of neutral density with the environment. Since validation data span laboratory and field experiments of a wide range of scales, comparisons are made for nondimensional variables. Figure 25.7 shows the decay of the centerline velocity u_c/U_0 and the bulk dilution S versus the distance from the source x/D (as for a jet discharge with $\sigma = 0$, $\theta = 0$). The model comparison is limited to the self-similar region beyond the ZOFE. Over this region, the model predictions track through the mean of the experimental data, and the scatter in measured data is typically ±5%. Because the model assumptions are wholly valid within all of the asymptotic regimes, model comparisons for pure plumes, wakes, line puffs, and line thermals show similar levels of agreement.
2. *Buoyant jet in stratification*: As a first example of a transitional regime, consider a buoyant jet in a quiescent reservoir with linear density stratification. The comparison in Figure 25.8 shows the predicted centerline trajectory and half-width overlain on line tracings from images of the laboratory dye studies for an inclined discharge in the x-direction ($\sigma = 0$ and $\theta = \pi/4$). $T = g_0'/(\varepsilon D)$ is the stratification parameter. Note that the simulation terminates at the start of the intermediate field as the jet undergoes rapid spreading and begins to violate the boundary layer approximation. The model accurately predicts the evolution in the jet-like region of the flow and the height of maximum rise.
3. *Buoyant jet in crossflow*: Another important transition region considers the buoyant jet in an unstratified crossflow. The dominant length scale for this case is L_b; Figure 25.9 presents the model validation for a vertically discharging jet ($\sigma = 0$ and $\theta = \pi/2$). From this log–log plot, it is apparent that the model captures the correct scale-law behavior in the weakly bent ($z \sim x^{3/4}$ power law) and strongly bent ($z \sim x^{2/3}$) regions. The model also tracks the experimental data throughout the near field, but slightly underpredicts the rise height (overpredicts the degree of bending) for $x/L_b > 100$. This is due to an overestimate of the drag force in the latest stages of the jet, indicating that the drag force term becomes less important as the jet transitions from a coherent column to a diffusion-dominated puff or thermal.
4. *Buoyant jet in stratified crossflow*: Among the more complicated cases that can be analyzed using the CorJet model equations is a buoyant jet into a flowing and density-stratified ambient reservoir. Figure 25.10 shows the case of a vertical buoyant jet ($\sigma = 0$ and $\theta = \pi/2$) into a uniform current with linear density stratification. In these experiments, the initial momentum was small so that the flow was dominated by the discharge buoyancy. The model predicts well the intrusion level of the plume and is particularly capable of matching the measured dilution, as indicated by the variation of ρ_c/ρ_a versus x/D. Again, the model simulation is terminated when the jet enters to collapsing region of the intrusion formation.

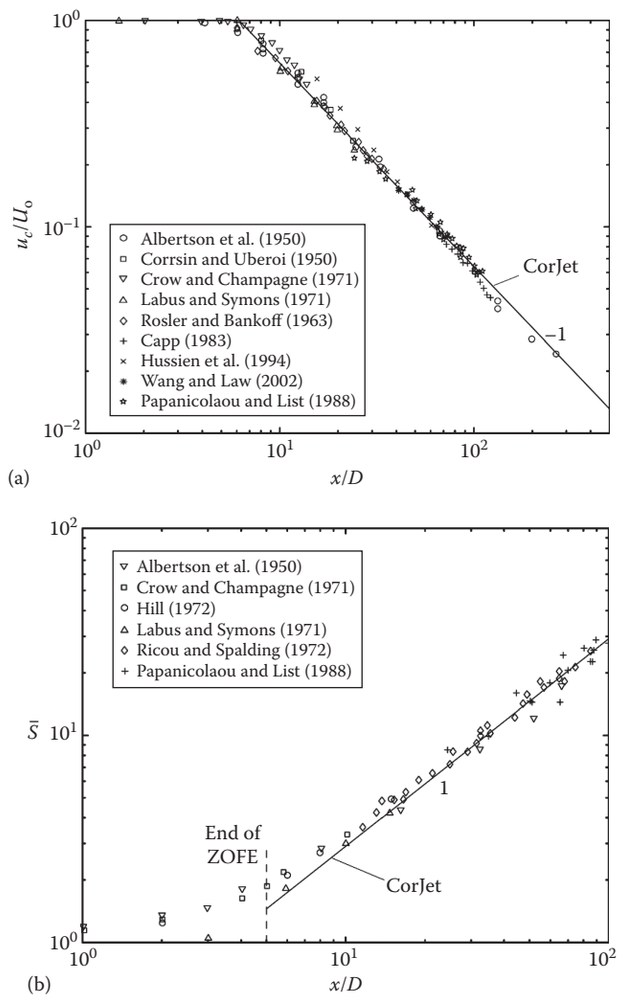

FIGURE 25.7 Validation of the pure jet showing the decay of the centerline velocity and the evolution of the bulk dilution as a function of nondimensional distance from the jet nozzle. (Reproduced from Jirka, G.H., *Environ. Fluid Mech.*, 4(1), 1–56, 2004. With permission.)

25.4 Applications

25.4.1 Discharge Analysis Using CORMIX

Environmental impact assessment is often required for a wide range of point source discharges—including municipal wastewaters, cooling waters, industrial wastes, oil, and gas produced waters, dredging operations, and desalination brines—into

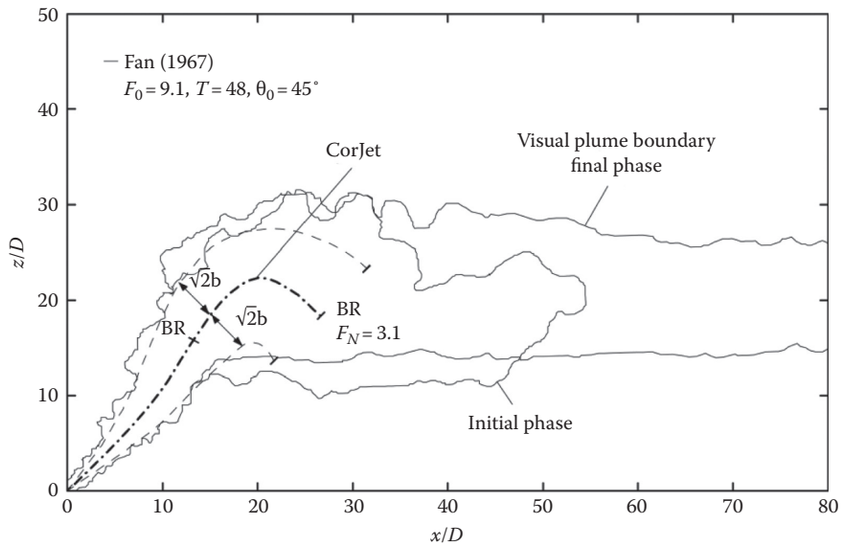

FIGURE 25.8 Validation of the trajectory and half-width for an inclined buoyant jet into a linearly stratified ambient reservoir. (Reproduced from Jirka, G.H., *Environ. Fluid Mech*., 4(1), 1–56, 2004. With permission.)

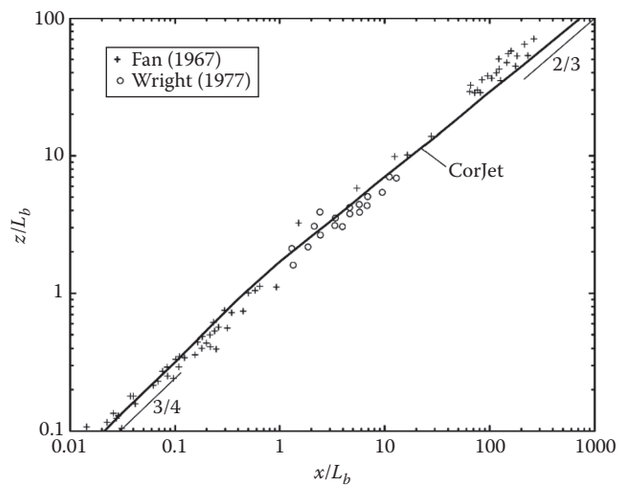

FIGURE 25.9 Validation of the trajectory for a buoyant jet in crossflow using the buoyancy length scale as the normalization parameter. (Reproduced from Jirka, G.H., *Environ. Fluid Mech*., 4(1), 1–56, 2004. With permission.)

rivers, lakes, estuaries, and the coastal ocean. Design optimization of wastewater disposal systems using multiport diffusers can often mitigate negative environmental impacts. Because of this, predictive simulation models are used to design, manage, and regulate wastewater disposal systems.

The previous sections outlined the physical concepts and theoretical basis for buoyant jet modeling into an unbounded (infinite) ambient. However, water bodies always have limitations; be it the surface, bottom, shorelines, or boundaries caused by internal ambient density stratification. This section addresses the practical application of buoyant jet modeling to water quality management within the regulatory mixing zone, where boundary interaction is often important. The regulatory mixing zone is an administrative concept which includes the region near the discharge where the initial mixing occurs and generally spans an area from the discharge through the intermediate field and to the start of the far field (refer to Figure 25.1). Although the potential for water quality impacts are greatest within the mixing zone, the opportunity also exists to mitigate adverse conditions through outfall design optimization.

The CORMIX modeling system (Version 6.0 or higher) is a software system for the analysis, prediction, and design of aqueous toxic or conventional pollutant discharges into diverse water bodies. It contains a buoyant jet integral model as previously described along with enhancements to account for boundary interaction within the mixing zone. The system emphasizes steady-state ($\partial Q/\partial t = 0$), near-field mixing and contains methods to predict conditions within the regulatory mixing zone which typically occurs after boundary interaction in the far-field region (where ambient conditions dominate mixing). While CORMIX was originally developed under the assumption of steady ambient conditions, Version 6.0 includes application to highly unsteady environments, such as tidal reversal conditions, in which transient recirculation and pollutant build-up effects can occur. Figure 25.11 gives the problem domain covered by the CORMIX methodology in relationship to ambient and discharge conditions.

Among available water quality simulation models, CORMIX has a unique data-driven approach to simulation model selection based primarily on the characteristic scales defined in the Dimensional Analysis section and on other similar scales for more complicated cases. To do this, CORMIX employs a rule-based expert system to screen input data and select the appropriate core hydrodynamic simulation model to simulate the physical mixing processes contained within a given

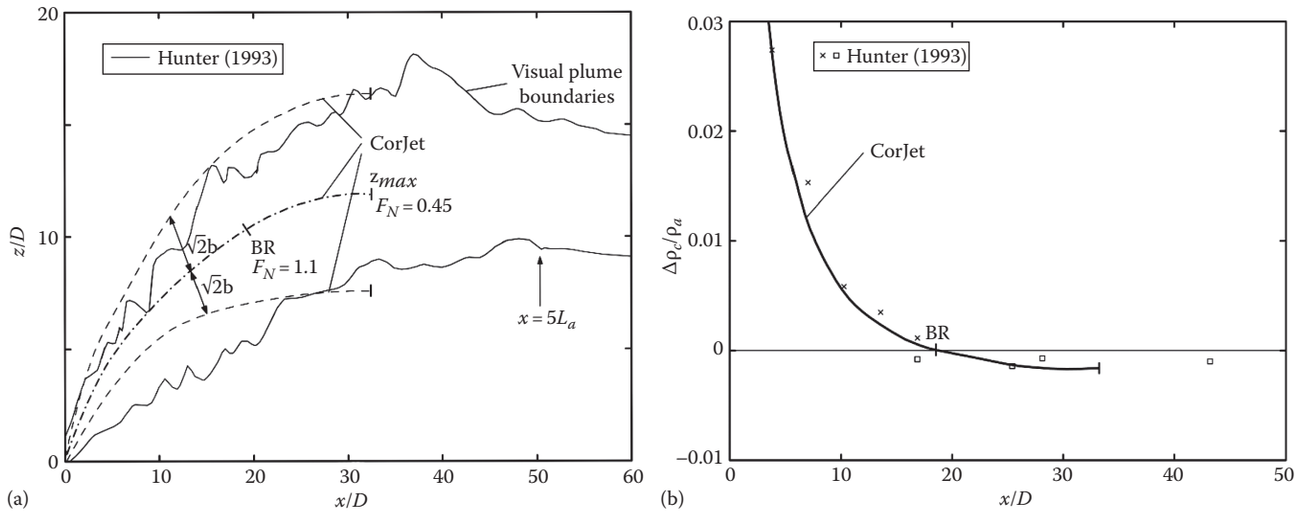

FIGURE 25.10 Validation of the buoyant jet in stratified crossflow showing the jet trajectory, half-width, and centerline decay of the density difference. (Reproduced from Jirka, G.H., *Environ. Fluid Mech.*, 4(1), 1–56, 2004. With permission.)

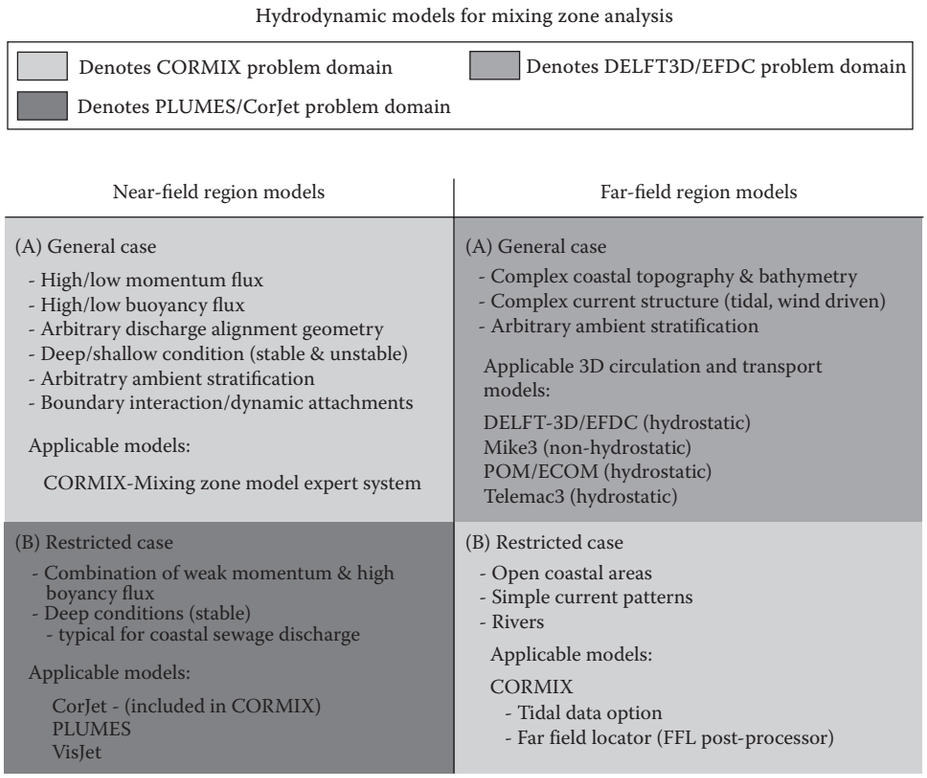

FIGURE 25.11 CORMIX mixing zone model problem domain.

discharge–environment interaction. The methodology also comprehensively documents the model selection process and interprets the physical mixing processes present in relation to applicable regulatory criteria. Since the model selection process is data-driven and explicitly contained within the methodology, the approach facilitates a discussion between regulators and the regulated on the physical processes contained within the mixing zone, limits the potential for model misapplication, and helps to develop consensus on appropriate model selection. Figure 25.12 shows an example of the CORMIX flow classification system based upon length scale analysis of the boundary interaction process. CORMIX determines discharge stability and

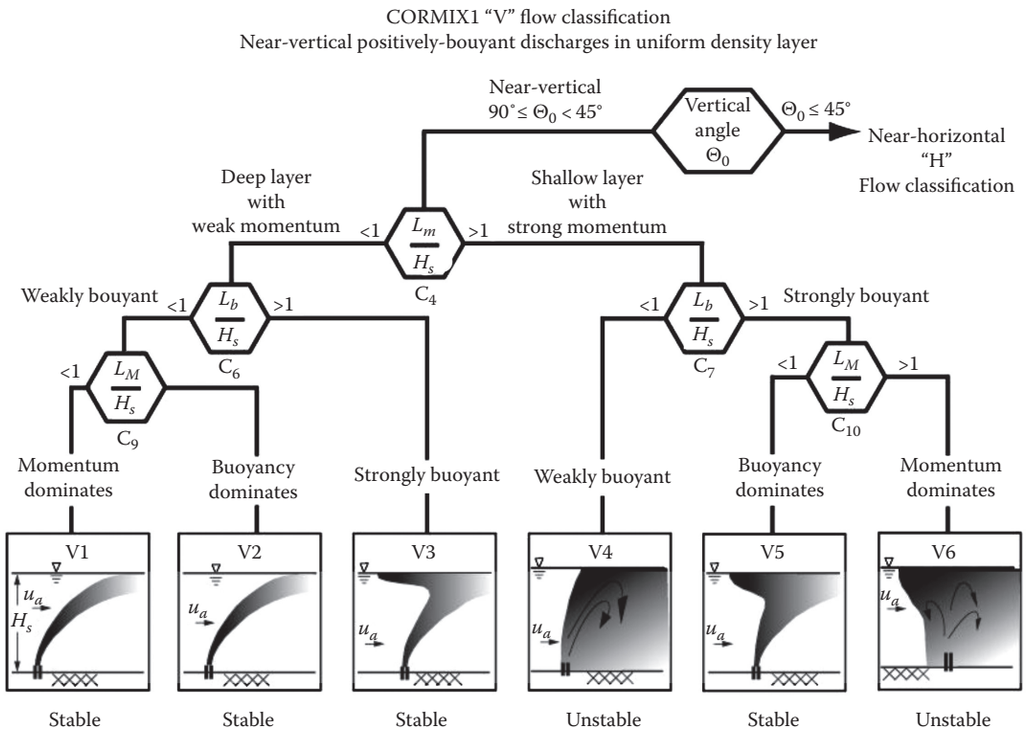

FIGURE 25.12 The CORMIX flow classification.

the boundary interaction process before executing a series of regional flow models to complete the near-field and far-field simulation. CORMIX also determines if dynamic wake or Coanda attachments occur in the near-field. The entire CORMIX system contains about 60 flow classifications similar to V1 to V6 in the figure.

A User Manual gives a comprehensive description of the CORMIX system (Doneker and Jirka 1990). Multiple publications describe the scientific basis for the CORMIX system and demonstrate comparison and validation with field and laboratory data (Akar and Jirka 1991; Bleninger et al. 2002; Doneker 2003, 2006; Doneker and Jirka 1990; Jones et al. 1996).

25.5 Extensions for Multiport Diffusers

For larger flow rates, single jet discharges may not be sufficient to achieve dilution requirements, for example, if applied for municipal treated wastewater effluent or cooling water discharges where large volume flow rates must be accommodated. Multiple jets, called multiport diffusers, are used in such cases to distribute the effluent through many single ports discharges along a diffuser pipe. Such diffusers can generally be modeled as a continuous line source, aligned at an oblique angle to the ambient current, discharging from a theoretical slot of finite length resulting in a plane jet (see Figure 25.13). Provided that the slot length is considerably larger than the local jet width, the resulting jet motion is then characterized by a locally 2D plane geometry. The overall behavior of the resulting jet motion (including its complete trajectory) may, however, still be 3D. Jirka (2006) described the extension from single jets to plane jets and the details of a plane jet integral model. The definitions conform to those given previously for the round jet geometry. In addition, there are the diffuser length L_D, port spacing l, port and diffuser orientations β, γ, θ, and the equivalent slot width B, calculated to achieve diffuser flux quantities equal to those caused by the sum of the individual multiport jets. The assumption of the equivalent slot width concept is generally valid for most of the existing closely spaced multiport diffuser installations, where merging takes place after short distances and in a rather uniform manner. Exceptions are for tunneled outfalls with only a few largely spaced long risers and rosette-like port arrangements. Individual jet quantities are then no longer the right measure for calculating the equivalent slot width and more complicated jet interactions must be considered.

Turbulent fluctuations caused by turbulence shearing mechanisms lead to a gradual growth of the characteristic jet thickness $2b$ and characteristic width $L_D + 2B$. The relatively large diffuser lengths compared to plume thickness $L_D/(2B)$?1 generally allow neglecting the entrainment at the lateral plume ends. Plane plume growth, thus, is dominated by 2D processes, and quantities per unit jet length can be described for the initial fluxes as (Jirka 2006) AQ4

$$q_0 = \frac{Q_0}{L_D} = U_0 B \tag{25.44}$$

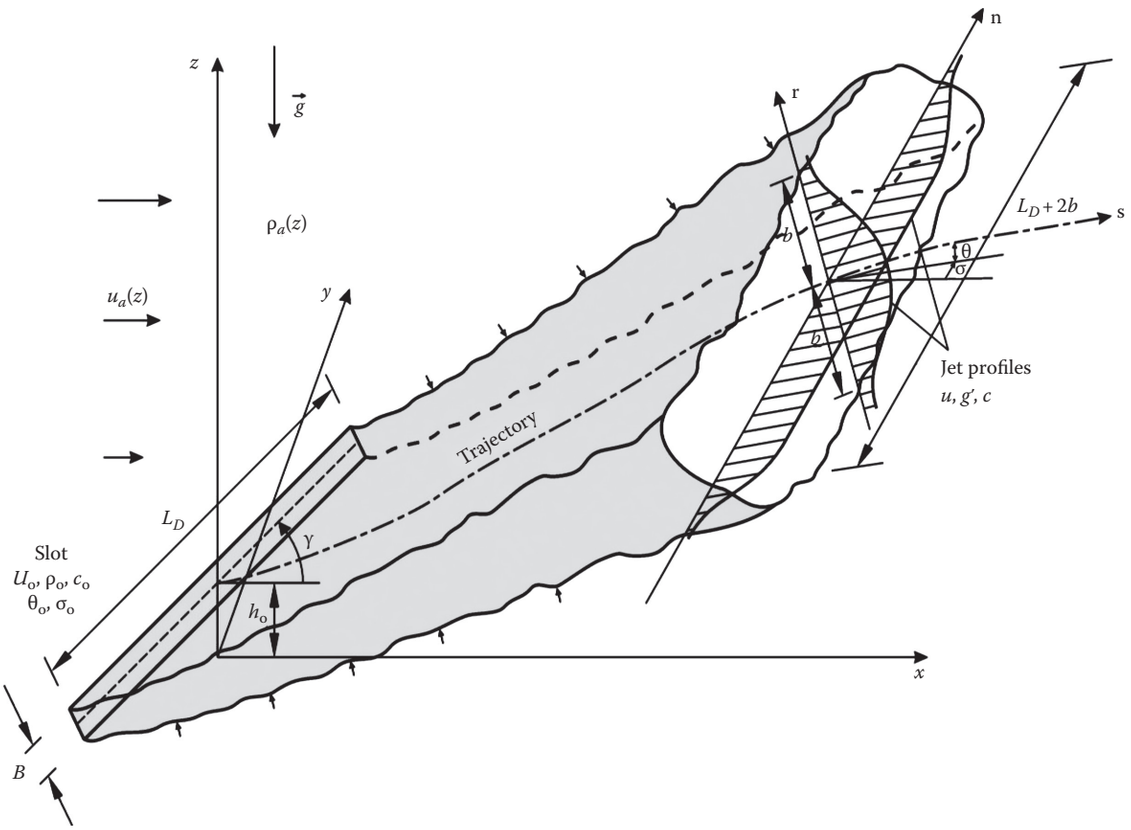

FIGURE 25.13 Schematization for merging jets discharged unidirectionally by multiport diffusers. (Reproduced from Jirka, G.H., *Environ. Fluid Mech*., 6(1), 43–100, 2006. With permission.)

$$m_0 = \frac{M_0}{L_D} = U_0^2\, B \tag{25.45}$$

$$j_0 = \frac{J_0}{L_D} = U_0 g_0' B \tag{25.46}$$

$$q_{c0} = \frac{Q_{c0}}{L_D} = U_0 c_0 B \tag{25.47}$$

The development of the plane jet fluxes q, m, and j along the centerline can be computed in integral values as described in Jirka (2006).

It has been demonstrated both theoretically and experimentally that the maximum mixing can be achieved with closely spaced ports that allow some interference of adjacent jets (Fischer et al. 1979). In relatively shallow coastal waters of typical depth 5–15 m, however, it is often the case that, given practical considerations (e.g., in order to maintain a minimum jet velocity and minimum diameter), multiport diffusers are designed to minimize interference of adjacent plumes. In such cases, the required spacing is about $H/3$.

25.5.1 Extensions for Surface Jets

Buoyant surface discharges occur in many environmental and water treatment processes, including inflows to treatment facilities, discharges to receiving bodies, and riverine inflows to larger rivers, lakes, of the coastal ocean. When lighter than the receiving water, the discharge forms a buoyant surface jet, as sketched in Figure 25.14, where a river discharges at an angle into a flowing coastal region.

Buoyant jet integral models have recently been adapted to accurately model the jet-like near field, the transition to plume-like buoyant spreading, and the buoyancy-dominated intermediate field. Jones et al. (2007) present scale relationship to classify the dominant inflow dynamics, and Jirka (2007) presents the integral model equations. A 3D numerical model with an imbedded surface jet are also presented by Hetland (2010) and Chen et al. (2009) and compared to field data of the Merrimack river plume near Boston, Massachusetts, by Hetland and McDonald (2008). Laboratory data are also available from Nash et al. (1995).

The general physics of a buoyant jet is analogous to the round jet detailed previously. An initial ZOFE takes place at the start of the jet as the nearly uniform velocity profile of the channel rapidly adapts to a nearly round jet with typical Gaussian profiles (though

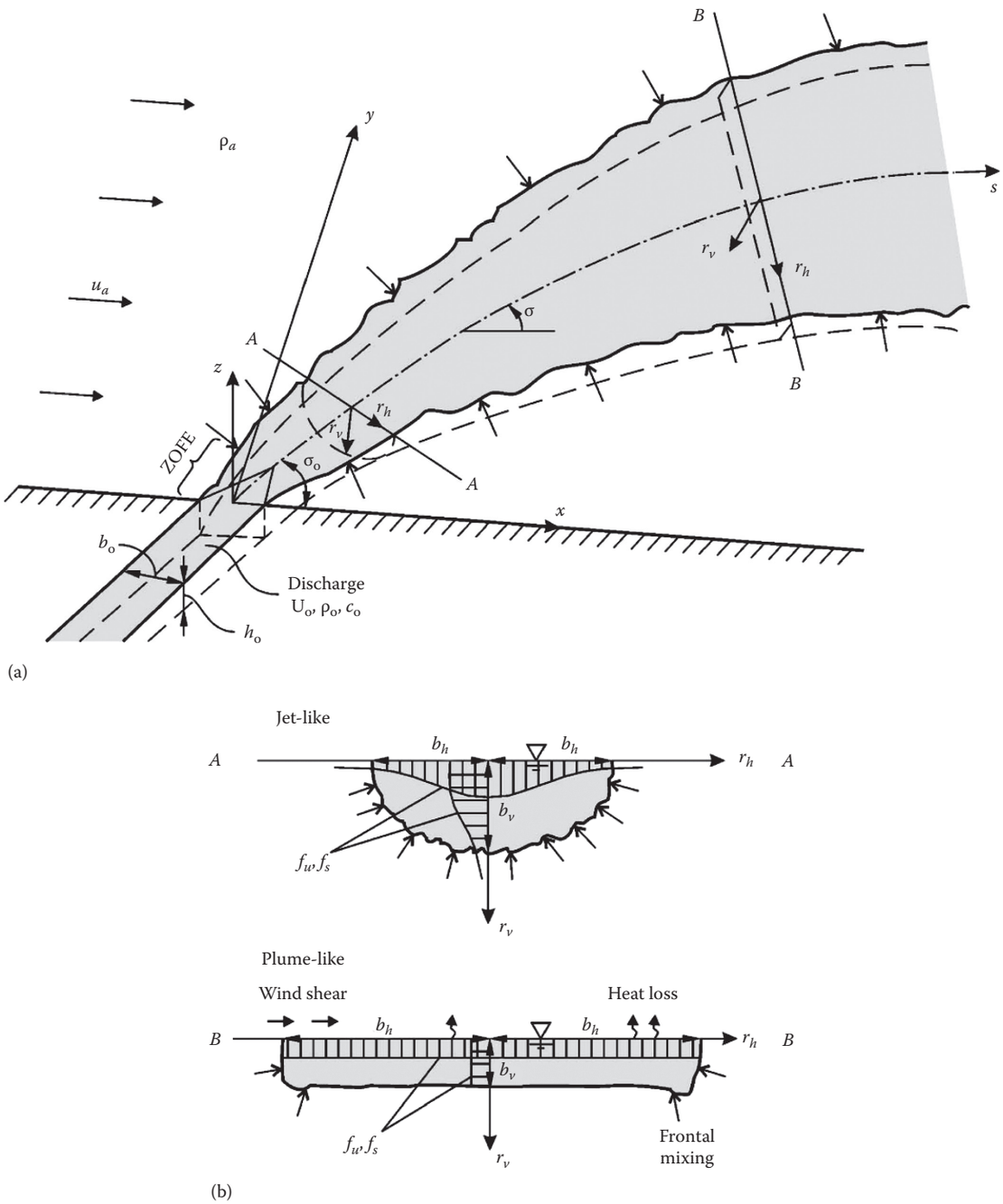

FIGURE 25.14 Schematic of a surface discharge: (a) perspective view and (b) cross sections. (Reproduced from Jirka, G.H., *J. Hydraul. Eng-Asce*, 133(9), 1021–1036, 2007. With permission.)

influenced by the surface as shown in inset A of Figure 25.14). As the jet flow slows down, buoyancy begins to dominate and the flow collapses to form a plume-like lateral intrusion. In this latter region, vertical diffusion is damped by density stratification on the bottom of the plume, and the velocity profiles steepen, approaching a more top-hat profile (see inset B of Figure 25.14). Wind shear can enhance mixing, and coastal currents can deflect the plume; eventually, the flow enters the far-field, where it is dominated by turbulent diffusion and passive advection.

Throughout the buoyant jet near and intermediate field, several different entrainment fluxes engulf ambient fluid. These rates are additive, and are summarized by

$$E = E_h + E_v + E_p + E_f + E_i$$

where the subscripts stand for horizontal, vertical, advected puff, frontal, and interfacial entrainment, respectively (Jirka 2007). E_h enters at the jet edges, depends on the centerline velocity, and is comprised of jet and wake entrainment. The vertical entrainment E_v on the jet bottom has a similar form to E_h, but with an added density term to account for damping at the sharp interface in the collapsed jet. As in the round jet, the advected puff entrainment E_p depends on the ambient velocity and the angle of the surface jet. In the plume region, an additional frontal entrainment E_f is proportional to the lateral spreading velocity of the surface plume sides. The final term E_i acts on the plume bottom, modeling the effect of wind mixing, and is proportional to the wind shear velocity, the ambient current velocity, and the lateral spreading. The drag force is also formulated similarly to that in a round jet, following a quadratic law drag model that depends on the ambient current velocity. No additional drag is modeled due to the wind since it is assumed that this effect is already included in the ambient current.

25.6 Challenges

Although an extensive and diverse range of buoyant jets types in the environment have been studied in great detail, as described briefly in this chapter and elsewhere, there are numerous challenges remaining to further our understanding and description of jets and plumes. A few of these challenges are highlighted as follows.

A rapidly expanding field of buoyant jet discharges result from membrane-based seawater desalination plants, and generate plumes with positive momentum and negative buoyancy, similar to a fountain. As long as the discharge angle is not vertical (which would violate principle 3 similarly to a jet in a counterflow), a buoyant jet following the boundary layer approximation results, and the equations presented earlier accurately track its trajectory from the source until it plunges to the sea floor, where boundary interaction dominates. There, the dense discharge interacts with the nonhorizontal sea bed and creates further gravity currents down slope, which need more detailed consideration than pure buoyant spreading processes at the water surface for positively buoyant effluents. A related desalination byproduct are thermal saline discharges resulting from distillation plants, where double diffusion effects may occur. Because these plumes interact with the flora and fauna of the sea floor, their environmental impact can be significant, and their design requires new models, experiments, and methods.

AQ5 Another challenge area in jets and plumes are those resulting from multiphase discharges, such as direct ocean CO_2 sequestration plumes, particle-laden jets from dredging operations or untreated wastewater discharges, lake aeration and mixing plumes, among others (see also Chapter 5 of *Handbook of Environmental Fluid Dynamics, Volume Two*). Because of the immiscibility of the phases, there exists the possibility that the entrained fluid separates from the dispersed phase (e.g., air, oil, liquid CO_2, sediment, etc.). And because the dispersed phase often contains much of the buoyancy in a multiphase jet, the result is a nonuniform loss of buoyancy to the jet as the dispersed phase settles or rises out of the jet, thus depleting the driving force of the jet motion. When separation of phases is weak, the integral approach described here can be effective; however, when separation is important (notably in the presence of crossflow or ambient stratification), new models are required. Because of the difficulty to make measurements in multiphase flows, data are often lacking for more complicated cases, and much work is needed to understand the fundamental flow dynamics.

Other ambient forcing conditions beyond those discussed here may also play a major role in some buoyant jet applications. These may include the influence of waves, ambient turbulence, counter flows, and others. These processes can affect both the jet trajectories and dilution. In many of these cases and also in cases of the other traditional flow classes as they interact with boundaries, no experimental data are available for model validation; hence, there remain many buoyant jet flow types that require fundamental observation in the laboratory. These may also be explored in the near future as numerical solutions can be increasingly applied to jets and plumes. Certainly, this field will be vibrant for years to come.

References

Akar, P. J. and Jirka, G. H. (1991). CORMIX2: An expert system for hydrodynamic mixing zone analysis of conventional and toxic submerged multiport diffuser discharges. *EPA-600/3–19/073*, USEPA, Athens, GA.

Bleninger, T., Lipari, G., and Jirka, G. H. (2002). Design and optimization program for internal diffuser hydraulics. *Proceedings of International Conference on Marine Waste Water Discharges 2002*, Istanbul, Turkey, pp. 16–20.

Chen, F., MacDonald, D. G., and Hetland, R. D. (2009). Lateral spreading of a near-field river plume: Observations and numerical simulations. *J. Geophys. Res. Oceans*, 114, 12.

Davidson, M. J. and Pun, K. L. (1999). Weakly advected jets in cross-flow. *J. Hydraul. Eng. ASCE*, 125(1), 47–58.

Doneker, R. L. (2003). Systems development for concentrate disposal: CorVue and corSpy interactive visualization tools for CORMIX mixing zone analysis. *Final Report No. 98*, U.S. Bureau of Reclamation, DSRP, Denver, CO.

Doneker, R. L. (2006). Systems Development for Environmental Impact Assessment of Concentrate Disposal: Development of Density Current Simulation Models, Rule Base, and Graphic User Interface. U. B. O. Reclamation, ed.

Doneker, R. L. and Jirka, G. H. (1990). CORMIX1: An expert system for mixing zone analysis of conventional and toxic single port aquatic discharges. *EPA-600/3–90/012*, USEPA, Athens, GA.

Doneker, R. L. and Jirka, G. H. (1991). Expert systems for mixing-zone analysis and design of pollutant discharges. *J. Water Res. Plann. Manage.*, 117(6), 679–697.

Doneker, R. L. and Jirka, G. H. (1998). *D-CORMIX: A Decision Support System for Hydrodynamic Mixing Zone Analysis of Continuous Dredge Disposal Sediment Plumes. American Society of Civil Engineers*, New York. AQ6

Doneker, R. L., Nash, J. D., and Jirka, G. H. (2004). Pollutant transport and mixing zone simulation of sediment density currents. *J. Hydraul. Eng. ASCE*, 130(4), 349–359.

Fan, L. N. (1967). Turbulent buoyant jets into stratified or flowing ambient fluids. Report No. KH-R-15, W.M. Keck Laboratory of Hydrology and Water Resources, California Institute of Technology, Pasadena, CA.

Fischer, H. B., List, E. J., Koh, R. C. Y., Imberger, J., and Brooks, N. H. (1979). *Mixing in Inland and Coastal Waters*. Academic Press, New York.

Görler, H. (1942). Berechnung von Aufgaben der freien Turbuleny aus Grund eines neuen Näherungsansatzes. *ZAMM*, 22, 244–254.

Hetland, R. D. (2010). The effects of mixing and spreading on density in near-field river plumes. *Dyn. Atmos. Oceans*, 49(1), 37–53.

Hetland, R. D. and MacDonald, D. G. (2008). Spreading in the near-field Merrimack River plume. *Ocean Model*, 21(1–2), 12–21.

Jirka, G. H. (2004). Integral model for turbulent buoyant jets in unbounded stratified flows. Part I: Single round jet. *Environ. Fluid Mech.*, 4(1), 1–56.

Jirka, G. H. (2006). Integral model for turbulent buoyant jets in unbounded stratified flows, Part 2: Plane jet dynamics resulting from multiport diffuser jets. *Environ. Fluid Mech.*, 6(1), 43–100.

Jirka, G. H. (2007). Buoyant surface discharges into water bodies. II: Jet integral model. *J. Hydraul. Eng. ASCE*, 133(9), 1021–1036.

Jirka, G. H. and Akar, P. J. (1991). Hydrodynamic classification of submerged single-port discharges. *J. Hydraul. Eng. ASCE*, 117(HY9), 1095–1111.

Jirka, G. H. and Doneker, R. L. (1991). Hydrodynamic classification of submerged single-port discharges. *J. Hydraul. Eng. ASCE*, 117(9), 1095–1112.

Jirka, G. H. and Lee, J. H. W. (1994). Waste disposal in the ocean. In: *Water Quality and Its Control*, Vol. 5, M. Hino, ed. A.A. Balkema Publishers, Rotterdam, the Netherlands.

Jones, G. R., Nash, J. D., Doneker, R. L., and Jirka, G. H. (2007). Buoyant surface discharges into water bodies. I: Flow classification and prediction methodology. *J. Hydraul. Eng. ASCE*, 133(9), 1010–1020.

Jones, G. R., Nash, J. D., and Jirka, G. H. (1996). CORMIX3: An expert system for mixing zone analysis and prediction of buoyant surface discharges. DeFrees Hydraulics Laboratory, Cornell University, Ithaca, NY.

Kundu, P. K. and Cohen, I. M. (2008). *Fluid Mechanics*, 4th Edn. Academic Press, New York.

Morton, B. R., Taylor, G., and Turner, J. S. (1956). Turbulent gravitational convection from maintained and instantaneous sources. *Proc. R. Soc. Lond. A Mat. Phys. Sci.*, 234(1196), 1–23.

Nash, J. D., Jirka, G. H., and Chen, D. (1995). Large-scale planar laser-induced fluorescence in turbulent density-stratified flows. *Exp. Fluids*, 19(5), 297–304.

Reichardt, H. (1941). Gestzmäßigkeiten der freien Turbulenzen. *VDI-Forschungsheft*, 414.

Schlichting, H. (1960). *Boundary Layer Theory*. McGraw-Hill Book Company, Inc., New York.

Tang, H. A., Paik, J., Sotiropoulos, F., and Khangaonkar, T. (2008). Three-dimensional numerical modeling of initial mixing of thermal discharges at real-life configurations. *J. Hydraul. Eng.*, 134(9), 1210–1224.

Tian, X. D. and Roberts, P. J. W. (2003). A 3D LIF system for turbulent buoyant jet flows. *Exp. Fluids*, 35(6), 636–647.

Tollmien, W. (1926). Berechnung turbulenter Ausbreitungsvorgänge. *ZAMM*, 6, 468–478.

Turner, J. S. (1986). Turbulent entrainment: the development of the entrainment assumption, and its application to geophysical flows. *J. Fluid Mech.*, 173, 431–471.

Wright, S. J. (1977). Mean behavior of buoyant jets in a crossflow. *J. Hydraul. Div. ASCE*, 103(HY5), 499–513.

Xiao, Y., Lee, J. H. W., Tang, H., and Yu, D. Y. (2005). Numerical study of multiple tandem jets in crossflow. *XXXI IAHR Congress*, Seoul, South Korea. AQ7

Yu, D. Y., Ali, M. S., and Lee, J. H. W. (2006). Multiple tandem jets in cross-flow. *J. Hydraul. Eng. ASCE*, 132(9), 971–982.

Author Queries

[AQ1] Please note that equations have been renumbered for sequential order. Please check.
[AQ2] Please check whether the insertion of "negative" is ok in the sentence "If the jet deviates …."
[AQ3] Please provide the description of part labels in the caption of Figure 25.10.
[AQ4] Please check the expression "L_D/(2B)?1" in the sentence "The relatively large diffuser…" for correctness.
[AQ5] Please check the inserted cross reference to chapter in the sentence "Another challenge area …." for correctness.
[AQ6] Please provide in-text citation for the following references: Doneker and Jirka (1998), Doneker et al. (2004), and Tang et al. (2008).
[AQ7] Please provide page range for reference Xiao et al. (2005).